Forward Model Studies of Water Vapor using Scanning Microwave Radiometers, Global Positioning System, and Radiosondes during the Cloudiness Inter-Comparison Experiment

Vinia Mattioli, *Member, IEEE,* Ed R. Westwater, *Fellow, IEEE,* Seth I. Gutman, and Victor R. Morris

Abstract—**Brightness temperatures computed from five absorption models and radiosonde observations were analyzed by comparing them with measurements from three microwave radiometers at 23.8 and 31.4 GHz. Data were obtained during the Cloudiness Inter-Comparison experiment at the U.S. Department of Energy's Atmospheric Radiation Measurement Program's (ARM) site in North-Central Oklahoma in 2003. The radiometers were calibrated using two procedures, the so-called instantaneous "tipcal" method and an automatic self-calibration algorithm. Measurements from the radiometers were in agreement, with less than a 0.4-K difference during clear skies, when the instantaneous method was applied. Brightness temperatures from the radiometer and the radiosonde showed an agreement of less than 0.55 K when the most recent absorption models were considered. Precipitable water vapor (PWV) computed from the radiometers were also compared to the PWV derived from a Global Positioning System station that operates at the ARM site. The instruments agree to within 0.1 cm in PWV retrieval.**

Index Terms— **GPS, microwave radiometry, microwave propagation, radiometric accuracy, water vapor.**

I. INTRODUCTION

GROUND-BASED microwave radiometers (MWRs) have been widely used to measure brightness temperatures (T_BS) to derive atmospheric precipitable water vapor (*PWV*) [1]–[3]. In particular, MWRs at 23.8 and 31.4 GHz have shown high reliability for the accurate estimation of this parameter [3], and they are currently operational at the U.S.

V. Mattioli is with the Department of Electronic and Information Engineering, University of Perugia, Perugia, 06125 Italy, (phone: +39-075-5853832; fax: +39-075-5853654; e-mail: mattioli@diei.unipg.it).

E.R. Westwater is with the Environmental Technology Laboratory, Cooperative institute for Research in Environmental Sciences, University of Colorado/NOAA, Boulder, CO 80305 USA (e-mail: Ed.R.Westwater@noaa.gov).

V.R. Morris is with the Department of Energy's Pacific Northwest National Laboratory, Richland, WA 99352 USA (e-mail: victor.morris@pnl.gov).

S.I. Gutman is with the GPS-Met Observing Systems Branch/NOAA Forecast Systems Laboratory, Boulder, CO 80305 USA (e-mail: Seth.I.Gutman@noaa.gov)

Department of Energy's Atmospheric Radiation Measurement Program (ARM) climate research facilities [2]. Additionally, the use of the Global Positioning System (GPS) for the measurement of *PWV* has generated great interest in recent years. This interest is due to the large number of available permanent stations and to low instrument and maintenance costs. Moreover, this technique allows data assimilation of *PWV* into operational weather forecasts [4].

Comparisons of *PWV* from MWR, GPS, and radiosondes (RAOBs) are described in [5], [6]. Inter-comparisons of *PWV* estimates from MWR with different techniques, including Raman lidar [7], satellite near infrared (IR) reflectance and IR emittance techniques [8] have also been made. All of these comparisons depend on the accuracy of the sensors and on the forward model used in deriving *PWV* from the MWR.

With the objective of developing and improving the accuracy of parameterizations describing atmospheric water vapor, clouds, and radiative transfer, a Cloudiness Inter-Comparison Intensive Operational Period (CIC-IOP) was conducted during March–April 2003 at the ARM Southern Great Plains Central Facility (SGP) in North-Central Oklahoma, USA. In particular, three MWRs at 23.8 and 31.4 GHz were continuously operated during the IOP. A SuomiNet GPS receiver was also operated. Moreover, radiosondes containing the Vaisala RS90 humidity sensor were launched four times a day. Standard ARM instruments included a Micropulse Lidar, a Millimeter Wave Cloud Radar (MMCR), and a suite of optical and infrared sensors [9], [10].

Utilizing these data, this work compares forward models in computing brightness temperature from RAOBs using data from the three MWRs. The data were screened for clear conditions using a variety of techniques, including lidar measurements. Two different tipping calibration algorithms were applied, the instantaneous tipcal calibration method [11] developed at the Environmental Technology Laboratory (ETL) and the ARM calibration algorithm [2]. In Section II the instruments used are described; in Section III the forward models, the MWR calibration, and the methodology for *PWV* retrievals are explained; in Section IV we present the radiometer data analysis, and in Section V we discuss the comparison of brightness temperature computed from the

models and RAOBs with the MWR measurements. Finally, in Section VI a comparison between *PWV* derived from GPS, MWR and RAOBs is discussed.

As mentioned above, there have been previous works comparing MWRs with radiosondes and GPS. However, our work contains several new results. First, we analyzed data from three simultaneous MWRs to insure strict quality control and calibration consistencies. We also compared, for the three MWRs, two calibration algorithms. Finally, in addition to the five absorption models, two of them being very recent, we had high-quality RS90 radiosonde data available. Because several previous results were based on Vaisala RS80 data that were known to have a dry bias [3], [12]–[13], the availability of the RS90 data is particularly significant.

The SGP site is an excellent facility for testing the performance of the models. Data available at this extensively monitored location [9] allowed us to overcome many problems that can be encountered in a less well-implemented site for which not all the instruments are available. The availability of active cloud-measuring instruments allow the data to be separated into clear and cloud categories, as well. A complete description of these sensors is available online at the ARM internet site [http://www.arm.gov/instruments/]. A long history of radiosonde observations also allows accurate modelling of water vapor retrieval coefficients. In addition, the SGP meteorology frequently exhibits large changes in water vapor in a relatively short time. Thus, for forward model studies involving water vapor, the site and its associated instrumentation are ideal.

II. INSTRUMENTS DEPLOYED DURING THE CLOUDINESS INTER-COMPARISON EXPERIMENT

During the CIC-IOP a variety of instruments were operating at SGP. In this section we describe those on which we focused our analysis.

The operational SGP Central Facility MWR, designated C1, is a dual-channel water vapor radiometer of the WVR-1100 series from Radiometrics [www.radiometrics.com] operating at 23.8 and 31.4 GHz. The half-power beam width of the two channels is 5.9 and 4.5 degrees, respectively. The C1 MWR scans at five elevation angles (19.35, 23.4, 30.15, 41.85 and 90.0 degrees) in an east-west direction during clear conditions, but shifts to the zenith-viewing Line Of Site (LOS) mode [http://www.arm.gov/instruments/static/mwr.stm] during cloudy conditions. Two MWRs of the same type, designated E14 and S01, supplemented the operational MWR for two months during the CIC-IOP. E14 scanned continuously (i.e., not shifting to the LOS mode during cloudy conditions) in the same vertical plane as that of operational unit, while S01 was scanning continuously in a north-south direction, orthogonal to the other two. The MWRs' elevation angles were set to be the closest to air masses 3, 2.5, 2, 1.5, and 1 (see Section III B).

A GPS permanent station, belonging to the SuomiNet network (site ID SG01) and managed by the University

Corporation for Atmospheric Research, is operating with collocated surface meteorological sensors at the SGP site. The antenna is a TRM33429.20+GP and the receiver type is a TRIMBLE 4700. The system is included in the NOAA/Forecast System Laboratory (FSL) Ground-Based GPS-IPW project [http://gpsmet.noaa.gov] network. To process the GPS data, FSL uses the GAMIT (GPS at Massachusetts Institute of Technology) software package [14] developed by MIT and Scripps Institution of Oceanography. Ultra-rapid orbits that are produced and updated hourly by the Scripps Institution Orbit and Permanent Array Center are used to derive *PWV* estimates every 30 minutes with less than 15-minute latency. The elevation cut-off angle was 7°.

Radiosondes of the Vaisala RS90 type [http://www.vaisala.com] were regularly launched four times a day (5.30, 11.30, 17.30, 23.30 UTC) at the SGP. The RS90 series contain the H-humicap relative humidity sensor, which consist of twin-heated sensors working in phase so that while one sensor is used for measuring, the other is heated.

Finally, we used a Vaisala CT25K ceilometer to determine clear-sky conditions overhead. A description of this instrument is given at [http://www.arm.gov/instruments/static/vceil.stm]. The instrument provides cloud information on a 15-s temporal scale, giving cloud base height with a 100-m range resolution, up to a nominal altitude of 25,000 ft (7.6 km). In some cases, data from ARM optical and infrared instruments, as well as data from the MMCR, were also used to identify clear skies.

III. METHODOLOGY

A. Clear-sky Forward Models

During clear conditions, the primary emitters of microwave thermal radiation in the troposphere are oxygen and water vapor, and the theory describing their absorption and emission has evolved continuously over the last 60 years. The quantity T_B is calculated from the Radiative Transfer Equation (RTE) [15], [16]. The RTE requires input values of vertical profiles of temperature $T(h)$ and absorption coefficient $\alpha(h)$, with h being the height above the surface. From a model of absorption, the absorption coefficient $\alpha(h)$ can be calculated as a function of frequency (and angle, for a stratified atmosphere) from measurements of vertical profiles of $T(h)$, pressure $P(h)$, and absolute humidity $\rho_V(h)$. In addition to T_B, the opacity τ, or total optical depth, is frequently used. It is related to T_B by

$$\tau = \ln\left(\frac{T_{mr} - T_c}{T_{mr} - T_B}\right) \qquad (1)$$

where $T_c = 2.75$ K is the T_B of the cosmic background, and T_{mr} is the mean radiating temperature. In this work, we compare measurements of T_B with calculations from three commonly used models: two were developed by Liebe and his colleagues [17]–[19] and the other by Rosenkranz [20], [21]. In addition

we compared two models that were recently developed, one by Rosenkranz [22] and its modification by Liljegren [23]. The improvements in [22] involved a modification of water vapor line intensities and pressure-broadened line shift of the 183.31 GHz water vapor line. The modification in [23] involved a 5% decrease of the self - and foreign-broadened line widths of the 22.345 GHz water vapor resonance as well as a change to the MT-CKD_ continuum [24]. For convenience, we will refer to these models as LIEB87, LIEB93, ROS98, ROS03 and LILJ04. In general, all of these models differ in the line-specific parameters such as line strength, self- and foreign-broadened line widths, as well as the so-called "continuum terms".

B. Calibration of the MWR

The general principles of calibration of microwave radiometers are well known [15], [16]. The specific calibration of the Radiometrics MWR is achieved by viewing a blackbody reference target at kinetic temperature T_{ref} both before and after noise from a diode has been injected into the signal. The sky equivalent T_B provided by the radiometer is given in [2]:

$$T_B = T_{ref} + \frac{f_w T_{nd}}{(V_{ref+nd} - V_{ref})}(V_{sky} - V_{ref}) \qquad (2)$$

where f_w is the polycarbonate foam window loss factor, T_{nd} is the noise diode injection temperature; V_{sky} and V_{ref} are the output signals when the radiometer is pointing at the sky and the reference target, respectively, and V_{ref+nd} is the signal when the radiometer is pointing at the reference target and the signal from the noise diode is injected. The quantity T_{nd} is determined by the tipcal method [25]. As explained in [25], a zenith scan is used to generate a curve of T_B vs. air mass, where air mass is defined as the ratio of the opacity at a direction θ and the opacity at zenith. The resulting curve, after $f_w T_B$ is converted to opacity, is known as a tip curve. The tipcal method adjusts T_{nd} such that $\tau(0) = 0$. In this work we evaluated two calibration methods for the MWRs, the ARM automatic self-calibration [2] and the ETL tipping calibration method [11]. The ETL method is based on instantaneous tip curves to derive for each tip the gain correction $f_w T_{nd}$ in (2). The measurements at angles on both sides of zenith are used to assure horizontal homogeneity under the assumption of a stratified atmosphere. The ARM calibration, in contrast, collects outputs of many tip curves (>500) satisfying the homogeneity condition during clear-sky conditions to linearly predict the noise diode injection temperature T_{nd} from the temperature of the blackbody target T_{ref}. Both calibration techniques were evaluated for clear-sky conditions in [26].

C. PWV from MWR

It is well known [1] that it is possible to retrieve water vapor and cloud liquid water from T_Bs measured by a ground-based MWR at 23.8 GHz and at 31.4 GHz. The first frequency is sensitive to the water vapor because of its proximity to the 22.235 GHz water vapor emission line, and it is chosen at the "hinge point" [27]. The other frequency, in contrast, in a clear-air window, is more responsive to the liquid water, because liquid water emits in a continuum increasing with frequency in this region of the spectrum. To retrieve water vapor and liquid water, T_Bs are usually converted into opacities τ_f as in (1) and PWV is then estimated by

$$PWV = a_0 + a_1 \tau_{23} + a_2 \tau_{31} . \qquad (3)$$

The retrieval coefficients a_i were estimated by linear regression for each month on the basis of ten years of RAOB data launched at the SGP.

D. PWV from the GPS

The excess path length (or GPS signal delay) introduced by the refractivity of the neutral atmosphere is estimated as a free parameter in the calculation of the GPS antenna position [28]. The GPS signal delay along a single slant path, is modeled in terms of an unknown zenith total delay (ZTD) and known elevation angle-dependent mapping functions as described by Niell [29]. Using the assumption that the total delay has only a hydrostatic component (ZHD caused by the mass of the atmosphere) and a wet component (ZWD caused by the dipole moment of the water vapor molecules along the paths of the GPS signals, we can establish the relationship:

$$ZTD = ZHD + ZWD . \qquad (4)$$

The ZHD is estimated from the atmospheric surface pressure measured at the height of the GPS antenna with high accuracy using the Saastamoinen model [30]; conversely, ZWD depends entirely on the moisture content of the atmosphere, and due to the highly variable humidity profiles, it is poorly predicted from surface measurements alone.

The ZWD is inferred by subtracting the ZHD from the ZTD, and then it is directly converted in PWV as in (5) by means of the coefficient π (see [31], [32]) given by (6):

$$PWV = \pi \cdot ZWD \qquad (5)$$

$$\pi = \frac{10^6}{\rho \cdot R_v \left[(k_3/T_m) + k_2' \right]} . \qquad (6)$$

The constants in (6) are k_2'=17 K·mb^{-1}, k_3=377.600 K^2·mb^{-1} [31], ρ is the density of liquid water, R_v is the specific gas constant for water vapor, and T_m [31] is the weighted mean temperature of the atmosphere:

$$T_m = \frac{\int (P_v/T)dz}{\int \left(P_v/T^2 \right)dz} \qquad (7)$$

where P_v is the partial pressure of water vapor and T is the

absolute air temperature. T_m is usually estimated from surface temperature T_S [33] because of the strong linear correlation between the two.

IV. RADIOMETER DATA ANALYSIS

A. Radiometer Comparisons

In this section, we present the comparison of the measurements from the three MWRs operating during the IOP, to evaluate their relative accuracy. One-minute averages of zenith measurements of T_Bs at 23.8 and 31.4 GHz by the three radiometers are compared in clear skies. Clear conditions were identified by using the ARM product from the Vaisala CT25K ceilometer. We evaluated MWR data measured during clear-sky conditions when the ceilometer was not indicating clouds for at least 20 minutes, centered on the radiometer data. Fig. 1 shows the analysis of T_Bs from the three MWRs for the measurement at 23.8 GHz, the MWRs being calibrated by the ETL algorithm. Fig. 1(a) is a plot of the T_B time series from the operational MWR C1 for the duration of the experiment and shows a range of about 40 K for the two-month duration of the experiment. Fig. 1(b) shows the T_B difference time series from MWRs S01 and E14 with respect to C1 and Fig. 1(c) shows the histograms of these differences. The average difference (bias) and standard deviation (std) are also reported. The same analysis for the measurements at 31.4 GHz is shown in Fig. 2. A summary of the statistical comparisons is given in Table I, which gives the comparisons of E14 and S01 with respect to C1, with T_Bs being calibrated by both the ETL and ARM algorithms. The slopes and intercepts of the regression line were computed relative to the C1 measurements. An agreement of the order of 0.3–0.4 K rms between the radiometers is evident from the table, showing that the radiometers are well calibrated. In addition, the slopes differ from unity by 2% error and the intercepts have a maximum absolute value of 0.4 K.

With three MWRs operating at the same time and at the same frequencies, we could also evaluate the performances of the wet window sensor mounted on the MWRs. The sensor turned the heater on during condensing or precipitating conditions to promote the evaporation of rain and snow. The sensor generally detected wet conditions correctly, but in some occasions the heater turned off too early or did not work during rain. For example, after a rainy event ended around 1400 UTC on April 19, the sensor worked properly for the S01 radiometer, turned off too early for the radiometer E14 (consequently the measurements were affected by droplets on the window for 15 minutes longer than were the S01 measurements) and did not heat the MWR C1 window, so that the measurements were affected for more than one hour. Nevertheless, other investigators [34] found that, on some occasions, the wet window sensor was too conservative. It is evident that having three nearly identical collocated MWRs allows for a variety of quality-control algorithms to be tested and evaluated.

B. Calibration Algorithm Comparison

For clear-sky cases we also compared the ARM and ETL calibration algorithms (see Fig. 3). Fig. 3(a) shows the T_B difference time series (ARM−ETL) for the two frequencies. Most of the differences between the two algorithms occurred after periods of rain or extended periods during which the instantaneous tipcal method could not be accurately applied. Histograms for the difference at 23.8 and 31.4 GHz are displayed in Fig. 3(b) and Fig. 3(c), respectively. The values of bias and std are also reported in the figures. Although the biases are small (0.16 K at 23.8 and 0.05 K at 31.4 GHz), we found an rms difference of the order of 0.4K for the 23-GHz measurement and of 0.3K for the 31-GHz measurement. The estimated accuracy of the ARM calibration in [2] is on the order of 0.2–0.3 K rms.

V. COMPARISON OF MODELS AND MEASUREMENTS

For each of the three radiometers and for each of the five absorption models of Section III.A, we compared measurements and calculations of T_B. Fig. 4 shows the T_B time series from the operational MWR C1 for the measurement at 23.8 GHz calibrated by the ARM algorithm and T_Bs computed from the RAOBs and the five models during clear-sky conditions from March 6 to March 11, 2003. Results of our comparisons are presented in Table II, in terms of bias and std. Two features are apparent:
1) For a given frequency, the std of the differences is relatively close (of the order of 0.1 K).
2) The results for the biases can be divided into roughly two classes; the first class is from the older models: LIEB87, LIEB93 and the second class from the newest models: ROS98, ROS03, and LILJ04.

As seen, the newest models are in much better agreement with the measurements. Finally, there appears to be slightly better agreement between measurements and ROS03 and LILJ04, although a larger data set would be necessary to choose the better model. Thus, for the newer models, the maximum bias is less than 0.55 K. We also note that, for a given radiometer, the difference between the ETL and ARM calibration is less than 0.1 K for the 31.4 GHz channel. We attribute the differences between radiometers to radiometer features that cannot be corrected by tipcal.

In addition to the statistical analysis shown in Table II, we also constructed scatterplots together with slope and intercept analyses of the regressions. In Fig. 5, we show these scatterplots of T_Bs from the MWR C1 calibrated by the ARM algorithm versus T_Bs computed from each of the five models. For the 23.8 GHz channel, there is about a 2.5 % difference in slope of ROS98/ROS03 calculations vs. that of LILJO4, with the two ROS calculations having a slope of nearly unity. The bias is nearly the same for the three newer models. For the 31.4 GHz channel, the LILJ04 is clearly in best agreement with a slope of nearly unity and an offset of nearly zero. The

slopes of ROS98/ROS93 are about 3.5 % different from unity and the magnitude of the offset is about 0.6 K.

VI. PWV DATA ANALYSIS

A. PWV: MWR vs. RAOB

It also was of interest to compare differences between the GPS, MWR and RAOBs in terms of their commonly derived parameter: PWV. In Table III we show the comparison of PWV retrieved from the MWRs and computed from RAOBs during clear-sky conditions. We have applied the retrieval coefficients derived from the ROS98, ROS03 and LILJ04 model computations to the T_Bs from the MWRs, which had provided the best results on the T_B comparisons (see Section V). The analysis is presented for both ARM and ETL calibration procedures. The comparison between MWRs and RAOBs shows good agreement in terms of bias (of the order of 0.02 cm) and std (less than 0.1 cm). Moreover, the three models produce similar results in terms of std, with a difference in terms of bias (of 0.03 cm) from LILJ04. We believe that the bias accuracies on the order of 0.02 cm reflect the high quality of the radiometers, the three models, and the RS90 humidity sensor.

B. PWV: MWR vs. GPS

In Table IV we show the comparison of PWV derived from the GPS as provided by the NOAA/FSL GPS-IPW project with PWV from the three MWRs. In the computation of the parameter π of (5) and (6), T_m is derived from the surface temperature T_S [33] measured by the collocated surface meteorological sensor. The comparison is performed using 30-minute-averaged MWR measurements centered on GPS data. The comparison shows very good agreement between PWV retrievals from MWRs and GPS, with an rms accuracy in general less than 0.1 cm. MWR S01 seems less in agreement with GPS relative to the other two MWRs, showing a bias of 0.02 cm in the PWV with respect to the PWV from MWR C1. Moreover, the use of coefficients derived from the LILJ04 model reduces the difference between PWV from MWR and GPS of the order of 0.03 cm in terms of bias. During clear sky conditions, the ETL calibration also reduced the bias between PWV from MWR and GPS on the order of 0.01 cm. In Fig. 6 the time series of PWV from MWR C1 (both calibrations applied), GPS, and RAOB are shown during clear-sky conditions from April 21 to April 23, 2003. The coefficients derived from the LILJ04 model were applied to T_Bs from C1.

We also evaluated the influence on the GPS PWV-estimation of the computation of T_m in the constant of proportionality π. In Table V we show the same comparison of Table IV, but with T_m computed as in (7) from the RAOBs. T_ms were interpolated to the same sampling time of GPS measurements. Our comparison shows that the computation of T_m from RAOBs improves the rms accuracy of PWV from the GPS on the order of 0.01 cm with respect to the MWR.

C. PWV: GPS vs. $RAOBs$

The comparison of PWV from the GPS with PWV from RAOBs is shown in Table VI. We evaluated PWV accuracy in the presence of clear air and clouds, again, with T_m estimated from T_S and computed from RAOBs. The comparison shows good agreement between PWV from the GPS and from RAOBs, with an rms on the order of 0.1 cm. We can notice that the use of T_m from RAOBs led to an improvement in the PWV rms accuracy on the order of 0.01 cm. This is consistent with our results for the same comparison with respect to the MWR. Clear and cloudy conditions were identified by using the ARM product from the Vaisala CT25K ceilometer at the SGP site. We classified clear-sky conditions when the ceilometer was indicating clear air for at least thirty minutes.

VII.   SUMMARY AND CONCLUSIONS

We have analyzed the results of five frequently used absorption models in terms of brightness temperature comparison with three microwave radiometers at 23.8 and 31.4 GHz operating during the Cloudiness Inter-Comparison experiment. We determined that the most recent models, ROS98, ROS03, and LILJ04 best fit the empirical data, with an average agreement at least as good as 0.55 K. Moreover, the three microwave radiometers have provided a very good data set for the analysis, with an agreement of the measurements on the order of 0.3–0.4 K rms when the ETL calibration procedure was applied. Radiometers and radiosondes have also shown a good agreement in terms of water vapor retrieval, with less than 0.12 cm rms difference. Using the LILJ04 model resulted in a bias, with respect to the radiosondes, of better than 0.06 cm. Our comparisons also demonstrated that the new Vaisala humidity sensor does not show the presence of the dry bias in the measurements of relative humidity.

In addition to bias and rms statistical analysis, we also constructed scatterplots together with slope and intercept analyses of the regressions. For the 23.8 GHz channel, there is about a 2.5 % difference in slope of ROS98/ROS03 calculations vs. that of LILJO4, with the two ROS calculations having a slope of nearly unity. The bias is nearly the same for the three newer models. For the 31.4 GHz channel, the LILJ04 is clearly in best agreement with a slope of nearly unity and an offset of nearly zero. The slopes of ROS98/ROS03 are about 3.5 % different from unity and the offset is about 0.6 K. For the 31.4 GHz channel, the LILJ04 is clearly in best agreement with a slope of nearly unity and an offset of nearly zero. The slopes of ROS98/ROS93 are about 3.5 % different from unity and the offset is about 0.6 K. In the LILJ04 model, both a 5 % decrease in water vapor line width from ROS98/ROS03 and a change in the continuum formulation were implemented. Our results suggest that the continuum formulation is a marked improvement, but that the 5 % line width implementation requires further study. This is important for the accurate remote sensing of water vapor and

cloud liquid water. Our results also show that the two older models LIEB87 and LIEB93 are at variance with the data.

The comparison of *PWV* from GPS with respect to MWR and RAOB also shows good agreement with an rms on the order of 0.1 cm. Still, we noticed that the GPS seemed to show a small bias during clear-sky conditions, of 0.04 cm less than *PWV* from RAOBs when T_m is derived from T_S. The same bias was observed in the comparison with the *PWV* retrieval from MWRs. However, the performance of the GPS retrievals during cloudy conditions (bias less than 0.004 cm) is very encouraging.

During the Cloudiness Inter-Comparison experiment, ARM SGP site provided an excellent facility for testing the performance of the models. The availability of three collocated MWRs allowed detailed accuracy comparisons in the measurement of brightness temperatures. The data from the GPS were useful in a variety of quality-control and instrument-comparison studies. The availability of active cloud-measuring instruments allowed the data to be separated into clear and cloud categories. A long history of radiosonde observations also allowed accurate modelling of water vapor retrieval coefficients. In addition, the SGP meteorology yielded large changes in water vapor during the two-month observation period. Thus, for forward model studies involving water vapor, the CIC experiment and its associated instrumentation were ideal.

Our focus in this paper has been on the analysis of water vapor measurements during clear sky conditions. Currently, for these conditions, the accuracy of PWV from the GPS measurement is limited by the accuracy of the total delay estimate and not on the meteorological errors associated with parsing the total delay into its wet and dry components, and mapping the wet component into precipitable water vapor. Maximum PWV errors associated with estimating the hydrostatic signal delay from surface pressure measurements with ~ 1 hPa accuracy is on the order of 0.3 mm. PWV errors associated with errors in estimating the parameter π from a surface temperature measurement with ~ 1deg K accuracy is approximately 0.1 mm.

The accuracy with which the total delay can be estimated is determined by the accuracy with which the position of the antenna (mostly the vertical coordinate) can be measured. In general, the position of an antenna can be measured with higher accuracy in shorter time using double-differencing techniques when stations are closely spaced. When stations are more widely spaced, it takes longer to resolve integer ambiguities and measurements made over the same period usually have higher uncertainty. In this sense, the most accurate measurements of PWV are made in places with the highest concentrations of GPS receivers, but other factors also contribute. These factors include the site environment (e.g.; obstructions, satellite visibility, degree of multipath, RF interference), stability of the antenna installation, antenna phase center model accuracy, and satellite orbit accuracy. As a consequence, and during clear sky conditions, we expect that the GPS PWV error caused by total delay estimation

errors and the process of retrieving PWV from the total delay will be on the order of 0.75 - 1 mm with only a minimal dependence on location.

Our ongoing research will examine the comparison between *PWV* from the GPS and from the MWR. We intend to explore the possible temperature dependence and the diurnal cycle, on both the MWR and the GPS measurements. The influence of satellite orbit errors will also be investigated. The precise GPS orbit information is available with 1–2 week latency from the International GPS Service for Geodynamics. Moreover, we recommend that MWR and forward model calculations be investigated for more extended periods of observations.

REFERENCES

[1] E.R. Westwater, "Ground-based Microwave Remote Sensing of Meteorological Variables," in *Atmospheric Remote Sensing by Microwave Radiometry*, M.A. Janssen, Ed. New York: J. Wiley & Sons, Inc, 1993, ch. 4, pp. 145–213.

[2] J.C. Liljegren, "Automatic self-calibration of ARM microwave radiometers," in *Microwave Radiometry and Remote Sensing of the Earth's Surface and Atmosphere*. Utrecht: P. Pampaloni and S. Paloscia, Eds., VSP Press, 2000, pp. 433–443.

[3] H.E. Revercomb, D.D. Turner, D.C. Tobin, R.O. Knuteson, W.F. Feltz, J. Bannard, J. Bosenberg, S. Clough, D. Cook, R. Ferrare, J. Goldsmith, S. Gutman, R. Halthorne, B. Lesht, J. Liljegren, H. Linne, J. Michalsky, V. Morris, W. Porch, S. Richardson, B. Schmid, M. Splitt, T. Van Hove, E. Westwater, and D. Whiteman, "The ARM programs's water vapor intensive observation periods: overview, initial accomplishments, and future challenges," *Bull. Amer. Meteorol. Soc.*, vol. 84, no. 2, pp. 217–236, Feb. 2003.

[4] D.E. Wolfe, S.I. Gutman, "Developing an operational, surface-based, GPS, water vapor observing system for NOAA: network design and results," *J. Atmos. Ocean. Technol.*, vol. 17, pp. 426–440, Apr. 2000.

[5] C. Rocken, T. Van Hove, J. Johnson, F. Solheim, R.H. Ware, M. Bevis, S. Chiswell, S. Businger, "GPS/STORM-GPS sensing of atmospheric water vapor for meteorology," *J. Atmos. Ocean. Technol.*, vol. 12, pp. 468–478, 1995.

[6] P. Basili, S. Bonafoni, R. Ferrara, P. Ciotti, E. Fionda, R. Ambrosini, "Atmospheric water vapour retrieval by means of both a GPS network and a microwave radiometer during an experimental campaign at Cagliari (Italy) in 1999", *IEEE Trans. Geosci. Remote. Sensing,* vol. 39, no. 11, pp. 2436–2443, 2001.

[7] Y. Han, J.B. Snider, E.R. Westwater, S.H. Melfi, R.A. Ferraro, "Observations of water vapor by ground-based microwave radiometers and Raman lidar," *J. Geophys. Res.*, vol. 99, no. D9, pp. 18 695–18 702, 1994.

[8] B-C. Gao, E.R. Westwater, B.B. Stankov, D. Birkenheuer, and A.F.H. Goetz, "Comparison of column water vapor measurements using downward-looking optical and infrared imaging spectrometry and upward-looking microwave radiometry," *J. Appl. Meteor.*, vol. 31, no. 10, pp. 1193–1201, Oct. 1992.

[9] T.P. Ackerman and G.M. Stokes, "The Atmospheric Radiation Measurement Program," *Physics Today*, vol. 56, no. 1, pp. 38–44, 2003.

[10] G.M Stokes and S.E. Schwartz, "The Atmospheric Radiation Measurement (ARM) Program: Programmatic background and design of the cloud and radiation tested," *Bull. Amer. Meteor. Soc.*, vol. 75, pp.1201–1221, 1994.

[11] Y. Han, E.R. Westwater, "Analysis and improvement of tipping calibration for ground-based microwave radiometers," *IEEE Trans. Geosci. Remote Sensing*, vol. 38, no. 3, pp. 1260–1276, 2000.

[12] J. Wang, H.L. Cole, D.J. Carlson, E.R. Miller, K. Beirle, A. Paukkunen, T.K. Laine, "Correction of humidity measurement errors from the Vaisala RS80 radiosonde-Application to TOGA COARE data," *J. Atmos. Ocean. Technol.*, vol. 19, pp. 981–1002, 2002.

[13] D. Cimini, E.R. Westwater, and B.M. Lesht, "Evaluation of recent improvements in humidity sounding by balloon-born sensors," in *2002 Proc. of the COST720 Workshop*, L'Aquila, June 19–21, 2002. [Available online: http://www.aquila.infn.it/people/Nico.Cimini.html/Reprints/Paper_COST720_RS90 _format.pdf].

[14] R.W. King and Y. Bock, "Documentation of the GAMIT GPS analysis software, version 9.4," Massachusetts Institute of Technology and Scripps Institution of Oceanography, 1996.

[15] M.A. Janssen, "An Introduction to the Passive Remote Sensing of Atmospheres," in *Atmospheric Remote Sensing by Microwave Radiometry*. New York: J. Wiley & Sons, Inc, 1993, pp. 1–36.

[16] F.T. Ulaby, R.K. Moore, and A.K. Fung, "*Microwave Remote Sensing, Active and Passive. Volume 1, Microwave Remote Sensing Fundamentals and Radiometry.*" Reading, Massachusetts: Addison-Wesley Publishing Company, 1981.

[17] H.J. Liebe and D.H. Layton, "Millimeter Wave Properties Of The Atmosphere: Laboratory Studies And Propagation Modeling," National Telecommunications and Information Administration (NTIA) Report 87-24, 1987, 74 pp. (available from the National Technical Information Service, 5285 Port Royal Road, Springfield, VA, 22161).

[18] H.J. Liebe, "MPM, An Atmospheric Millimeter Wave Propagation Model," *International Journal of Infrared and Millimeter Waves*, vol.10, no. 6, pp. 631–650, 1989.

[19] H.J. Liebe, G.A. Hufford, and M.G. Cotton, "Propagation modeling of moist air and suspended water/ice particles at frequencies below 1000 GHz," *AGARD conference proceedings* 542, 3.1–3.10, 1993.

[20] P.W. Rosenkranz, "Water Vapor Microwave Continuum Absorption: A Comparison Of Measurements And Models," *Radio Sci.,* vol. 33**,** no. 4, pp. 919–928, 1998.

[21] P.W. Rosenkranz, Correction to "Water Vapor Microwave Continuum Absorption: A Comparison Of Measurements And Models," *Radio Sci.*, vol. 34, no. 4, p. 1025, 1999.

[22] P.W. Rosenkranz, Massachusetts Institute of Technology, Cambridge, MA, private communication, March 2004.

[23] J.C. Liljegren, "Improved retrievals of temperature and water vapor profiles with a twelve-channel radiometer," in *2004 Proc. of the Eighth Symposium on IOAS-AOLS*, American Meteorological Society, 11–15 Jan. 2004, Seattle, WA.

[24] E. J. Mlawer, S. A. Clough, and D. C. Tobin, "The MT-CKD water vapor continuum: a revised perspective including collision induced effects," *Atmospheric Science from Space using Fourier Transfer Spectrometry (ASSFFS) Workshop*, 8-12 October 2003, Bad Wildbad (Black Forest) Germany.

[25] D.C. Hogg, M T. Decker, F.O. Guiraud, K.B. Earnshaw, D.A. Merritt, K.P. Moran, W.B. Sweezy, R.G. Strauch, E.R. Westwater, and C.G. Little, "An automatic profiler of the temperature, wind and humidity in the troposphere," *J. Appl. Meteor.*, vol. 22, no. 5, pp. 807–831, 1983.

[26] D. Cimini, E.R. Westwater, Y. Han, S.J. Keihm, "Accuracy of ground-based microwave radiometer and balloon-borne measurements during the WVIOP2000 field experiment," *IEEE Trans. Geosci. Remote Sensing,* vol. 41, no.11, pp. 2605–2615, Nov. 2003.

[27] J. Askne and H. Nordius, "Estimation of tropospheric delay for microwaves from surface weather data," *Radio Sci*, vol. 22, pp. 379–386, 1987.

[28] J. Marshall, M.S. Schenewerk, R. Snay, and S. Gutman, "The effect of the MAPS weather model on GPS-determined ellipsoidal heights," GPS Solutions, 5(1), pp. 1–14, 2001.

[29] A.E. Niell, "Global mapping functions for the atmospheric delay at radio wavelengths," *J. Geophys. Res.*, vol. 101, pp. 3227–3246, 1996.

[30] J. Saastamoinen, "Atmospheric Correction for the Troposphere and Stratosphere in Radio Ranging of Satellites," *The Use of Artificial Satellites for Geodesy*, vol. 15, S.W. Henriksen *et al.*, Eds., Geophysics Monograph Series, A.G.U., Washington, D.C., 1972.

[31] J.L. Davis, L.T.A. Herring, I.I. Shapiro, A.E. Rogers, and G. Elgered, "Geodesy by radio interferometry: Effects of atmospheric modelling errors on estimates of baseline length," *Radio Sci.*, vol. 20, pp. 1593–1607, 1985.

[32] M. Bevis, S. Businger, S. Chiswell, T.A. Herring, R.A. Anthes, C. Rocken and R.H. Ware, "GPS meteorology: mapping zenith wet delays onto precipitable water," *J. Appl. Meteor.*, vol. 33, pp.379–386, 1994.

[33] M. Bevis, S. Businger, T.A. Herring, C. Rocken, R.A. Anthes, and R.H. Ware, "GPS meteorology: remote sensing of atmospheric water vapor using the Global Positioning System," *J. Geophys. Res.*, vol. 97, pp. 787–801, 1992.

[34] D. Cimini, CETEMPS, University of L'Aquila, L'Aquila, Italy, private communication, April 2004.

Vinia Mattioli (M'04) was born in Perugia, Italy, in 1972. She received her M.S. in Electronic Engineering from the University of Perugia, Perugia, Italy in 2000. She is currently pursuing the Ph.D. degree in Information Engineering at the University of Perugia, Perugia, Italy.

Between 2003 and 2004 she spent 11 months at the Environmental Technology Laboratory, National Oceanic and Atmospheric Administration, Boulder, Colorado, USA, working on radiometer calibration, mathematical retrieval methods and GPS applied to atmospheric remote sensing. During this period she also participated in the 2004 Artic Winter Radiometric Experiment that was held in Barrow, Alaska, USA.

Ed R. Westwater (SM'91–F'01) was born in Denver, Colorado, in 1937. Currently, he is a Research Associate with the Cooperative Institute for Research in the Environmental Sciences, University of Colorado/National Oceanic and Atmospheric Administration, and is associated with the Microwave System Development Division of the Environmental Technology Laboratory/NOAA, in Boulder, Colorado. He received his B.A. degree in Physics and Mathematics from Western State College of Colorado in 1959, his M.S. in Physics in 1962 and his Ph.D. in Physics in 1970 from the University of Colorado.

He was employed by the U. S. Department of Commerce from 1960 to 1995, and joined CIRES in 1995. His research has been concerned with microwave absorption in the atmosphere, remote sensing of the ocean surface, microwave and infrared radiative transfer, ground- and satellite-based remote sensing by passive radiometry, and in the application of mathematical inversion techniques to problems in remote sensing. He has authored or coauthored 257 publications.

Dr. Westwater is a Fellow of the Institute of Electrical and Electrical Engineers (elected 12/3/2000) and received the 2003 Distinguished Achievement Award from The IEEE Geoscience and Remote Sensing Society. He is also a member of the American Meteorological Society, the American Geophysical Union, the Mathematical Association of America, is past Chairman of URSI Commission F (2000-2002), and served as Associate Editor of Radio Science (1999-2002). He presented the American Meteorological Society's Remote Sensing Lecture in 1997 and received 15th V. Vaisala Award from the World Meteorological Society in 2001. He was the Chairman and Organizer of 1992 International Specialists Meeting on Microwave Radiometry and Remote Sensing Applications and was a co-organizer of the Specialist Conference on Microwave Remote Sensing'01. He also served as a Guest Editor of the TGARS Special Issue devoted to Microrad 04.

Seth I. Gutman is Chief of the GPS-Met Observing Systems Branch of the NOAA Forecast Systems Laboratory in Boulder, Colorado.

He graduated from the University of Arizona in 1972 and has co-authored 13 peer-reviewed journal articles on GPS Meteorology since 1999.

Victor R. Morris was born in Spokane, Washington in 1958. He received his B.S. degree in Atmospheric Sciences from the University of Washington (UW) in 1982 and has obtained graduate studies in Computer Science and Environmental Sciences from Washington State University.

He was employed by the UW Astronomy Department in Seattle from 1980 to 1983 and joined the Pacific Northwest National Laboratory (PNNL) in Richland, Washington in 1983. Currently, he is a Technologist in PNNL's Atmospheric Sciences and Global Change Division of the Fundamental Science Directorate.

Mr. Morris specializes in the installation, operation, and maintenance of field measurement systems for meteorological, climatological, and wind energy research. He currently serves as the instrument mentor of the microwave radiometers, infrared thermometers, and total sky imagers for the U.S. Department of Energy's (DOE) Atmospheric Radiation Measurement program. His research has been concerned with wind turbulence characteristics and resource assessment for wind energy applications; measurements of atmospheric chemistry and aerosols from a research aircraft facility; and measurements of precipitable water vapor, cloud-base temperature, and cloud-fraction imagery at climate research facilities. He has authored or coauthored 18 publications. Mr. Morris received the Federal Laboratory Consortium Award for Excellence in Technology Transfer in 1994 from the U.S. DOE. He is a member of the American Wind Energy Association.

TABLES AND FIGURES

TABLE I
RADIOMETER T_B COMPARISON
$T_B(MWR)-T_B(C1)$

ETL calib.	Bias (K)	Std (K)	Slope	Intercept (K)
T_B(S01-C1) 23 GHz	0.27	0.28	0.984	0.079
T_B(E14-C1) 23 GHz	-0.22	0.21	1.009	0.027
T_B(S01-C1) 31 GHz	0.14	0.13	1.008	-0.258
T_B(E14-C1) 31 GHz	0.26	0.10	1.009	0.391
ARM calib.				
T_B(S01-C1) 23 GHz	0.29	0.27	0.989	-0.033
T_B(E14-C1) 23 GHz	-0.29	0.37	1.017	-0.101
T_B(S01-C1) 31 GHz	0.16	0.23	0.996	-0.099
T_B(E14-C1) 31 GHz	0.18	0.23	0.980	-0.104

Table I. Microwave radiometer comparisons. Sample size is 19078. Bias and std are referred to $T_B(MWR)-T_B(C1)$.

TABLE II
MODEL T_B COMPARISONS
$T_B(MWR)-T_B(RAOB)$

	ROS98		ROS03		LILJ04		LIEB87		LIEB93	
	Bias (K)	Std (K)	Bias (K)	Std (K)	Bias (K)	Std (K)	Bias (K)	Std (K)	Bias (K)	Std (K)
C1 ETL 23 GHz	0.24	0.75	0.18	0.75	-0.27	0.79	0.39	0.76	-0.85	0.93
C1 ARM 23 GHz	0.44	0.73	0.38	0.73	-0.07	0.76	0.60	0.73	-0.65	0.89
C1 ETL 31 GHz	-0.005	0.32	-0.05	0.33	-0.21	0.31	0.54	0.30	-0.86	0.51
C1 ARM 31 GHz	0.09	0.33	0.04	0.34	-0.11	0.30	0.64	0.31	-0.77	0.53
S01 ETL 23 GHz	0.52	0.60	0.45	0.60	0.004	0.62	0.67	0.60	-0.57	0.73
S01 ARM 23 GHz	0.75	0.70	0.69	0.70	0.25	0.71	0.91	0.69	-0.33	0.81
S01 ETL 31 GHz	0.13	0.27	0.07	0.27	-0.08	0.24	0.67	0.24	-0.72	0.49
S01 ARM 31 GHz	0.26	0.35	0.21	0.35	0.05	0.33	0.80	0.33	-0.59	0.52
E14 ETL 23 GHz	-0.03	0.77	-0.10	0.77	-0.55	0.82	0.12	0.79	-1.13	0.97
E14 ARM 23 GHz	0.15	0.88	0.08	0.89	-0.37	0.93	0.30	0.90	-0.95	1.08
E14 ETL 31 GHz	0.22	0.34	0.17	0.34	0.01	0.31	0.76	0.31	-0.64	0.54
E14 ARM 31 GHz	0.27	0.38	0.22	0.38	0.06	0.36	0.81	0.36	-0.59	0.53

Table II. Microwave radiometer T_Bs compared with T_Bs from RAOBs. Sample size is 67 for the comparison with MWR C1, 78 with S01,and 75 with E14. Bias and std are referred to $T_B(MWR) -T_B(RAOB)$.

TABLE III
PWV COMPARISON:
MWR-RAOB

	ROS98		ROS03		LILJ04	
ETL calib	Bias (cm)	Std (cm)	Bias (cm)	Std (cm)	Bias (cm)	Std (cm)
MWR C1	0.013	0.066	0.011	0.067	-0.020	0.074
MWR S01	0.031	0.050	0.030	0.051	-0.001	0.057
MWR E14	-0.025	0.076	-0.026	0.068	-0.056	0.076
ARM calib						
MWR C1	0.025	0.065	0.023	0.065	-0.007	0.073
MWR S01	0.046	0.055	0.045	0.056	0.014	0.062
MWR E14	-0.011	0.090	-0.012	0.082	-0.043	0.089

Table III. Microwave radiometer PWV compared with RAOBs. Sample size is 67 for the comparison with MWR C1, 78 with S01,and 75 with E14. Bias and std are referred to $PWV(MWR)-PWV(RAOB)$.

TABLE IV
PWV COMPARISON:
MWR-GPS (T_m FROM T_S)

	ROS98		ROS03		LILJ04	
	Bias (cm)	Std (cm)	Bias (cm)	Std (cm)	Bias (cm)	Std (cm)
C1 ETL	0.061	0.061	0.059	0.061	0.029	0.061
C1 ARM	0.073	0.065	0.072	0.064	0.041	0.063
S01 ETL	0.082	0.062	0.080	0.061	0.050	0.059
S01 ARM	0.096	0.065	0.095	0.064	0.064	0.062
E14 ETL	0.029	0.057	0.028	0.057	0.000	0.059
E14 ARM	0.038	0.063	0.037	0.063	0.008	0.065

Table IV. *PWV* from MWRs compared with *PWV* from GPS. Sample size is 826 for the comparison with MWR C1, 968 with S01,and 928 with E14. Bias and std are referred to *PWV*(MWR) -*PWV*(GPS). In the parameter π, T_m is computed from T_S.

TABLE V
PWV COMPARISON:
MWR-GPS (T_m FROM RAOBs)

	ROS98		ROS03		LILJ04	
	Bias (cm)	Std (cm)	Bias (cm)	Std (cm)	Bias (cm)	Std (cm)
C1 ETL	0.048	0.056	0.047	0.056	0.017	0.059
C1 ARM	0.060	0.059	0.059	0.059	0.029	0.060
S01 ETL	0.067	0.056	0.066	0.055	0.036	0.055
S01 ARM	0.082	0.060	0.080	0.059	0.050	0.058
E14 ETL	0.016	0.054	0.014	0.054	-0.015	0.058
E14 ARM	0.024	0.062	0.023	0.063	-0.007	0.066

Table V. *PWV* from MWR compared with *PWV* from GPS. Sample size is 826 for the comparison with MWR C1, 968 with S01, and 928 with E14. Bias and std are referred to *PWV*(MWR) -*PWV*(GPS). In the parameter π, T_m is computed from RAOBs.

TABLE VI
PWV FROM GPS COMPARED WITH RAOBs
PWV(RAOB)-*PWV*(GPS)

	Clear Sky		Cloudy		All	
	Bias (cm)	Std (cm)	Bias (cm)	Std (cm)	Bias (cm)	Std (cm)
*PWV*_GPS (T_m from T_S)	0.042	0.087	-0.003	0.115	0.016	0.104
*PWV*_GPS (T_m from RAOB)	0.027	0.073	-0.004	0.105	0.008	0.091

Table VI. *PWV* from GPS compared with *PWV* from RAOB. Sample size is 82 for the comparison during clear-sky conditions, 113 for the comparison during cloudy conditions, and 195 for the ensemble. Bias and standard deviation are referred to *PWV*(GPS)-*PWV*(RAOB).
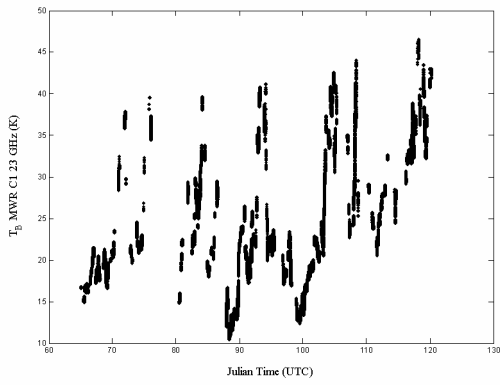
Fig.1(a)
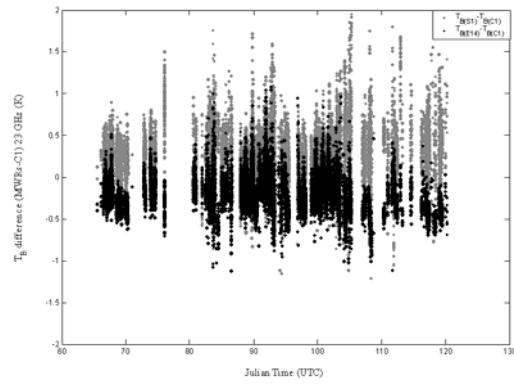
Fig.1(b)
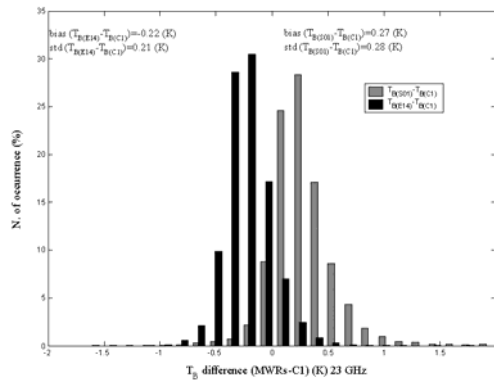
Fig.1(c)

Fig. 1. Analysis of T_B from MWR for the measurement at 23.8 GHz during clear-sky conditions. (a) T_B time series from the MWR C1 for the duration of the experiment. (b) T_B difference time series from MWRs S01 and E14 with respect to C1. (c) Histograms of the T_B differences from MWRs S01 and E14 with respect to C1. Bias and std are also reported.
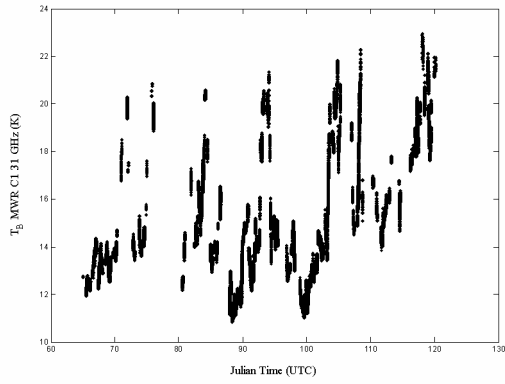
Fig.2(a)
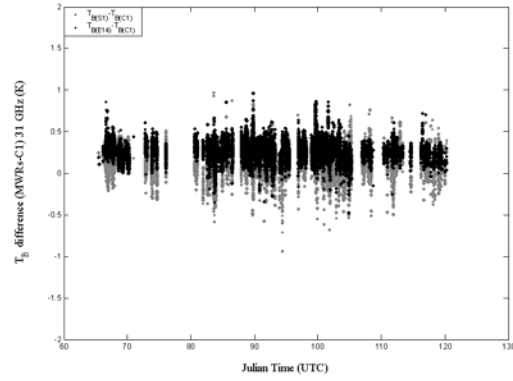
Fig.2(b)
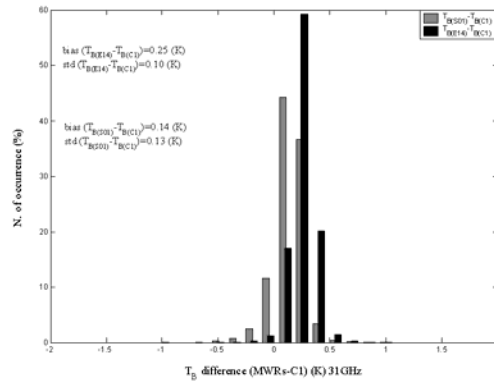
Fig.2(c)

Fig. 2. Analysis of T_B from MWR for the measurement at 31.4 GHz during clear-sky conditions. (a) T_B time series from the MWR C1 for the duration of the experiment. (b) T_B difference time series from MWRs S01 and E14 with respect to C1. (c) T_B differences from MWRs S01 and E14 with respect to C1. Bias and std are also reported.
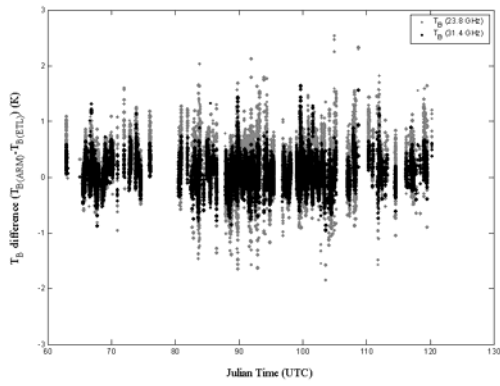
Fig.3(a)
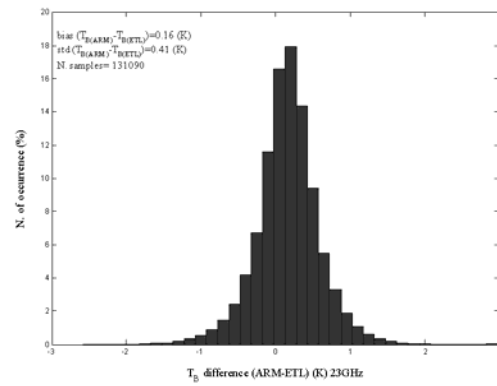
Fig.3(b)
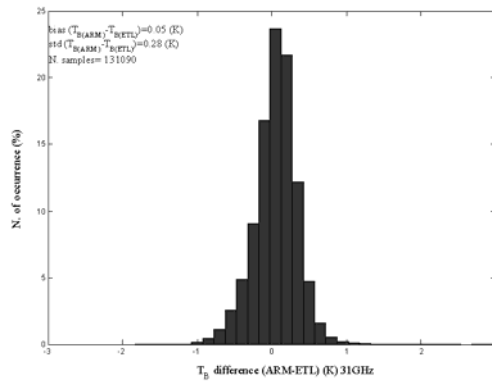
Fig.3(c)

Fig. 3. Comparison of the ARM and ETL calibration algorithms during clear-sky conditions. (a) T_B difference time series (ARM-ETL) for the two frequencies. (b) Histogram for the difference at 23.8 GHz. The value of bias and std are also reported. (c) Histogram for the difference at 31.4 GHz.
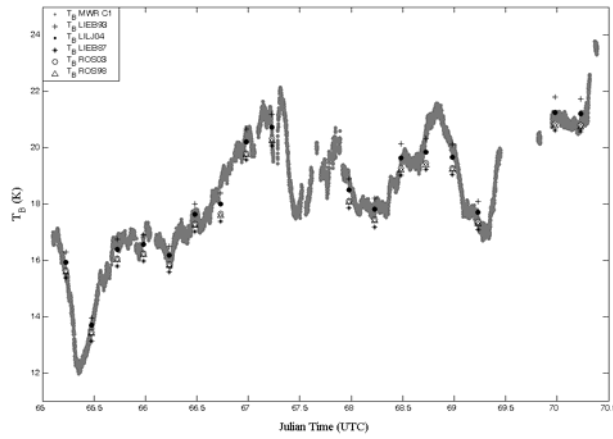
Fig. 4. T_B time series (gray dots) from the MWR C1 at 23.8 GHz (ARM calibration algorithm applied) and T_B computed from the RAOBs and the models LIEB87 (asterisks), LIEB93 (crosses), ROS98 (open triangles), ROS03 (white circles) and LILJ04 (black circles) during clear-sky conditions from March 6 to March 11, 2003.
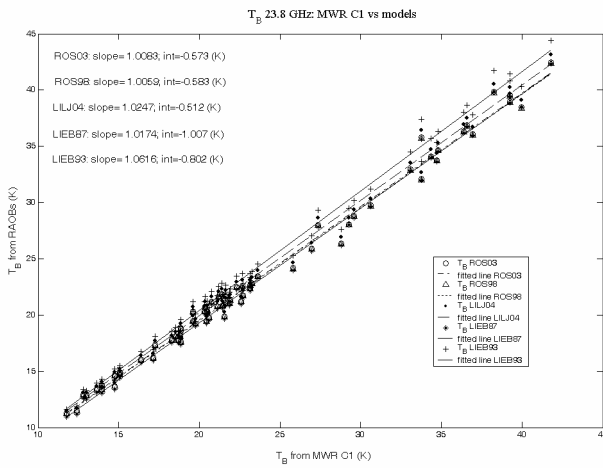
Fig.5(a)
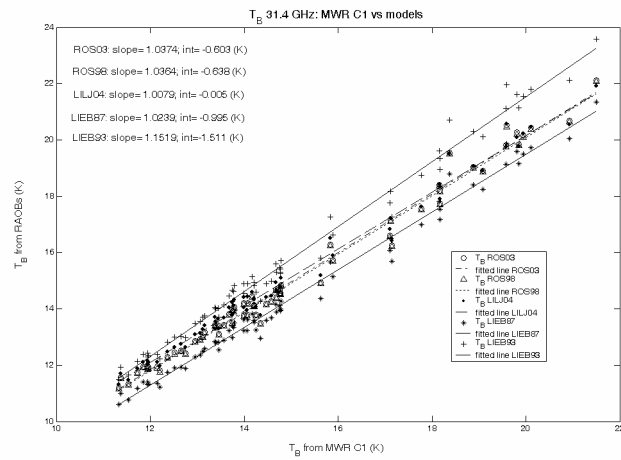
Fig.5(b)

Fig. 5. Scatterplots of T_Bs from the MWR C1 (ARM calibration algorithm applied) versus T_Bs computed from the RAOBs and the models LIEB87 (asterisks), LIEB93 (crosses), ROS98 (open triangles), ROS03 (white circles) and LILJ04 (black circles) during clear-sky conditions. The slopes and intercepts (int) of the regression line relative to the C1 measurements are also computed. Sample size is 67. (a) Scatterplot of T_B at 23.8 GHz. (b) Scatterplot of T_B at 31.4 GHz.
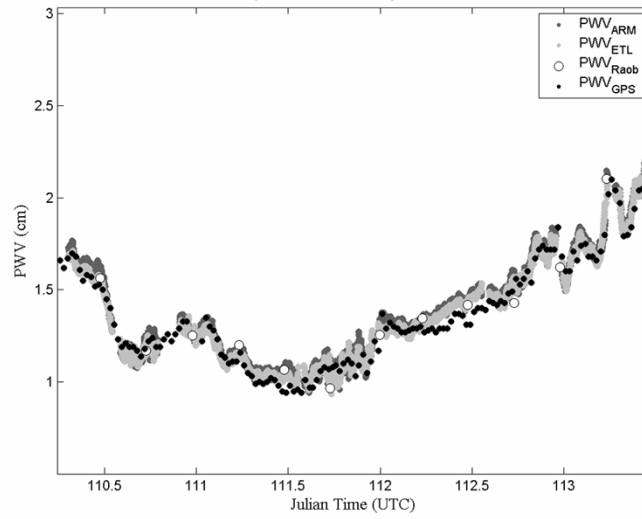
Fig. 6. Time series of *PWV* from MWR C1, ARM calibration (gray dots) and ETL calibration (light gray dots), *PWV* from GPS (black dots) and *PWV* from RAOBs (white circles) during clear-sky conditions from April 21 to April 23, 2003.